Analytical and Experimental Investigation of Entrainment in Capillary Pumped Wicking Structures

B. H. Kim
Research Assistant,
Department of Mechanical Engineering.

G. P. Peterson
Tenneco Professor and Head
of Mechanical Engineering,
Mem. ASME

K. D. Kihm
Assistant Professor of Mechanical
Engineering,
Mem. ASME

Department of Mechanical
Engineering,
Texas A&M University,
College Station, TX 77843

Analytical and experimental investigations were conducted to identify and better understand the parameters that govern the entrai»ment of liquid droplets in highvelocity gas streams flowing over capillary wicking structures. Using a flow visualization technique, two modes of entrainment were identified and described for high-velocity gas flows over an intermittently interrupted liquid surface. These two modes, roll-wave entrainment and stripping entrainment, were found to correspond to the lower and upper critical gas velocities, respectively. Measurements of the critical gas velocities and the droplet size distribution (Sauter mean diameter) of the entrained sprays were made as a function of the capillary pore size for three different mesh sizes and were compared with several analytical models developed in precious investigations. The flow visualization results indicate that the upper critical velocity is insensitive to variations in the capillary pumping rate provided the capillary pores are properly primed. The experimental results also indicate that the critical velocity for a given mesh is strongly influenced by the mesh dimensions, but that the previously developed criteria for estimating the critical velocity results in an underestimation of the upper critical velocity for all but very small pore sizes. Finally, to resolve this problem a new analytical model for predicting the critical velocity was developed and shown to be accurate for a wide range of capillary pore sizes.

Introduction

Many types of two-phase heat transfer devices used in the energy, chemical and petrochemical industries utilize a wicking structure to promote the flow of liquid from a condenser region back to the evaporator (Peng et al., 1992). Typically, these systems, which include transpiration coolers, distillation equipment, heat pipes, thermosyphons and capillary pumped systems, require that the liquid and vapor streams flow in either a parallel or countercurrent direction. At high thermal powers, the vapor velocities in these devices may reach the critical velocity, causing liquid droplets to be stripped or torn off the liquid surface and entrained in the vapor flow (Peterson, 1986). Once this entrainment occurs, the amount of liquid being returned may be depleted, resulting in either partial or complete dryout of the region where vaporization occurs. In an effort to identify and better understand the parameters that govern the entrainment of liquid droplets in these types of applications, a combined analytical and experimental investigation of the entrainment of liquid droplets in air/vapor streams flowing over screen mesh interfaces was undertaken.

In many types of two-phase heat transfer devices, the vapor velocity can be related to the axial heat transport by means of an energy balance. In this way, the critical vapor velocity, i.e., the velocity at which entrainment occurs, can be expressed as a function of the maximum thermal transport capacity, q_c, based upon the so-called entrainment heat flux limitation.

$$U_c = \frac{q_c}{\rho_v A_v h_{fg}} \tag{1}$$

This energy balance equation gives a reasonably accurate expression by which the critical velocity can be obtained, provided that the entrainment limit heat flux is known a priori. As noted by Peterson and Bage (1991), because of the difficulties associated with the measurement of the axial heat transport in these types of devices, prediction of the critical velocity using the entrainment heat flux limitation have not proven reliable in past studies, and only a limited amount of information about this limit is available in the literature.

The current investigation utilizes an experimental device similar to one first employed by Matveev et al. (1977), to provide an aerodynamic simulation of the entrainment occurring in screen mesh interfaces or capillary-driven devices, but differs from that of previous investigations in that measurements of both the critical velocity and droplet size distributions of the entrained sprays have been made as functions of the air/vapor

Contributed by the Petroleum Division for publication in the Journal of ENERGY RESOURCES TECHNOLOGY. Manuscript received by the Petroleum Division, May 19, 1992; revised manuscript received April 29, 1993. Associate Technical Editor: G. M. Reistad.

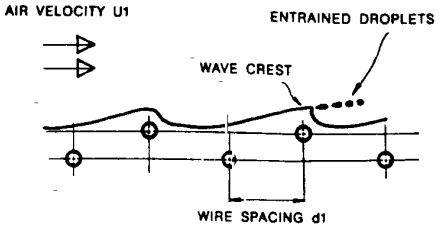

(a) Roll-wave entrainment (first mode)

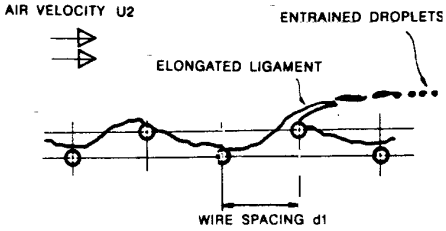

(b) Stripping entrainment (second mode)

Fig. 1 Two different modes of entrainment

velocities and the capillary pore size. The overall objectives of this investigation were to, first, experimentally establish and verify the relationship between the critical velocity and capillary pore diameter; and to, second, experimentally determine the Sauter mean diameter (SMD) variation as a function of both gas velocity and the wicking structure geometry.

Background and Literature Review

Prior to the formal investigation described herein, preliminary studies of the entrainment occurring in high-speed air/vapor flows were observed using a high-speed cinematographic recording technique. The results of these preliminary investigations indicated that two modes of entrainment occur for gas flows over an intermittently interrupted liquid surface. These two modes-roll-wave entrainment, referred to as the first mode of entrainment, and stripping entrainment, referred to as the second mode-are illustrated in Fig. 1, and correspond to the lower and upper critical velocities, respectively. Careful observation indicated that when a wicked surface was fully flooded, droplets are initially generated in the vicinity of the roll-wave crest, as shown in Fig. 1(a). While at this velocity, referred to as the lower critical velocity, droplets can be observed visually due to the scattering of a laser light beam, the mean diameters of the droplets typically are not measurable due to the small volume concentrations. As the air velocity increases, the wicked surface approaches a properly primed condition and long ligaments begin to form at the top of the roll-wave crests. In this transition region, the mode of entrainment begins to change, with the entrained droplets resulting not only from droplets off the roll-wave crest, but also from disintegration of the elongated ligaments. Further increases in the air velocity cause the whole menisci to become elongated and result in a periodic burst of entrained droplets due to the complete disintegration of the elongated ligaments, as shown schematically in Fig. 1(6). In this second mode, or stripping entrainment, the volume concentration of the periodic spray is high enough to be detected using Malvern particle sizing techniques. In addition to the disintegration of the elongated ligaments, the possibility of secondary breakup occurring as a result of aerodynamic shattering of the drops formed by stripping entrainment may occur.

Critical Velocity. Although helpful in understanding the entrainment phenomena, most of the previous investigations of entrainment in capillary-driven devices have not included modeling of the liquid vapor flow fields occurring at the wicked interface, and as a result, have been directed at measurement and prediction of the entrainment occurring in the first mode, or roll-wave entrainment using entrainment models for twophase annular flow (Ishii and Grolmes, 1975; Kataoka et al., 1983). For stripping entrainment, Cotter (1967) was the first to address the concept of the critical velocity in operating heat pipes using the surface instability theories developed by Kelvin and Helmholtz (Lamb, 1945)

$$\lambda_c = \frac{2\pi\sigma}{\rho_v U_c^2} \tag{2}$$

where λ_c, is the critical wavelength of a capillary wave. Using this expression and the characteristic wick dimension, L_c, in place of the critical wavelength, a critical velocity was derived as

$$U_c = \left(\frac{2\pi\sigma}{\rho_v L_c}\right)^{1/2} \tag{3}$$

In 1981, an experimental investigation was conducted to

Nomenclature

A_v = cross-sectional area of vapor flow (m^2)
δA_s = change of surface area (m^2)
c_1 = correlation const
C_D = drag coefficient
d = characteristic diameter (m)
d_l = wire spacing (m)
d_{21} = Sauter mean diameter (μm)
d_h = hydraulic diameter of wick pore (m)
D_h = duct hydraulic diameter (m)
d_m = mean diameter of wick pore(m)
d_{md} = volume median diameter(μm)
d_P = droplet diameter (μm)
d_{crit} = critical droplet diameter (μm)
e^+ = roughness Reynolds no.
f = friction factor
F_o = surface tension force (N)
FD = form drag force (N)
FS = frictional drag force (N)
$G(d_P)$ = cumulative distribution function
h_{fg} = latent heat of vaporization (kJ/kg)
I = light intensity
I_o = reference light intensity
K = dimensionless parameter
L_c = characteristic wick dimension(m)
Oh = Ohnesorge no.
P_{cm} = maximum capillary pressure(pa)
p_l = liquid pressure (Pa)
P_v = *vapor* pressure (Pa)
q_c = critical axial heat transport (W)
R^+ = modified roughness function
Re = duct Reynolds no. of vapor flow
Re^+ = roughness Reynolds no.
Re_c = critical Reynolds no.
Re_j = jet Reynolds no. based on droplet diameter
SMD = Sauter mean diameter (μm)
U = mean vapor velocity (m/s)
δV = volumetric change (m^3)
We = Weber no.
α = wave no., $2\pi/\lambda$ (m^{-1})
λ = wavelength (m)
τ = interfacial shear stress(N/m^2)
ρ = density (kg/m^3)
μ = viscosity (Pa-s)

Subscripts

c = critical values
l = liquid phase
v = vapor phase

determine the performance limits of gravity-assisted heat pipes with simple wick structures (Prenger and Kemme, 1981). It was concluded in this investigation that for entrainment to occur, the surface of the capillary wicking structure must be flooded allowing the interfacial meniscus to assume a convex shape, and implying that the liquid pressure must be greater than the vapor pressure for entrainment to occur. Using the criteria suggested by Busse and Kemme (1980), the flooded condition will occur only when the maximum capillary pressure, P_{cm}, is greater than the difference between the vapor and liquid pressures, i.e.,

$$| P_v - P_l | \leq P_{cm} \tag{4}$$

where the vapor pressure, P_v is equal to the sum of both the static and dynamic pressures, ($P_{vs} + \rho_v U^2/2$).

In addition to these theoretical investigations, Matveev et al. (1977) conducted an experimental investigation to measure the critical velocity of high-speed gas flowing over very fine mesh screens. The experimental results were compared with the values predicted by Eq. (3), utilizing the wire spacing, d_l, as the characteristic dimension. The results correlated reasonably well with the model, but only very small mesh sizes were evaluated. Busse and Kemme (1980) re-evaluated Cotter's initial formulation, and by comparing the magnitudes of the wavelength, λ, and the hydraulic diameter of the wick pore, d_h determined that entrainment would only occur for cases where the wavelength was much smaller than the capillary pore size, i.e., $\lambda \ll d_h$, unless the wick is fully flooded.

Another technique developed for predicting the onset of entrainment is the Weber number criteria (Peterson and Bage, 1991). In this technique, the Weber number is defined as the ratio of the shear force developed by the gas or vapor stream flowing over the capillary structure and the surface tension occurring at the liquid/vapor interface. This method assumes that the onset of entrainment occurs when the Weber number is equal to unity.

$$We = (\rho_v U^2 d_h / \sigma) = 1 \tag{5}$$

From this expression, the limiting vapor velocity can be obtained as

$$U_c = (\sigma / \rho_v d_h)^{1/2} \tag{6}$$

where d_h, is the hydraulic diameter of a characteristic wick pore.

Yet another approach to predict the critical velocity for fine meshes was proposed by Rice and Fulford (1987), who assumed that the principal pressure difference between the liquid and the vapor is due to the kinetic head of the vapor flow. By comparing the energy of formation, $\sigma \delta A_s$, and the energy required to create a pressure drop, $\Delta P \delta V$, the following criteria was proposed:

$$U_c = (8\,\sigma / \rho_v d_l)^{1/2} \tag{7}$$

As mentioned previously, a majority of the investigations conducted thus far have been directed at the first mode of entrainment in two-phase annular flow. Several additional studies, however, have addressed the second or stripping ertrainment mode, which would occur in a screen mesh interface subjected to high interfacial shear stresses. The stripping en trainment, however, has not been investigated in terms o1critical velocities and entrained droplet diameters.

Droplet Generation Mechanism. Previous investigations by Lane (1951) and Richardson (1989) have indicated that once liquid droplets have been entrained into a gas or vapor stream, they may break up into smaller droplets. The breakup or dis-integration of droplets in a moving gas or vapor stream is closely related to the drag force occurring on the surface due to the relative velocity between the gas and droplets. When this drag force becomes large enough to overcome the surface tension forces, the droplets disintegrate or break up into finer droplets. The criteria for this breakup, referred to as secondary breakup, is usually expressed as a function of the Weber number. Brodkey (1967) proposed the following correlation to derive the critical Weber number for such a flow condition by modifying a semi-empirical correlation between the critical Weber number and the viscosity group, developed by Hinze (1955), to obtain:

$$We_{crit} = 12 + 14\left(\frac{\mu_l^2}{\rho_v d_p \sigma}\right)^{0.8} \tag{8}$$

If the critical Weber number is assumed to have a value of approximately twelve, which is true for slightly viscous liquids such as water (i.e., the second term becomes negligible), then the critical diameter can be expressed as

$$d_{pcrit} = 12\sigma / \rho_v U_r^2 \tag{9}$$

where U_r represents the relative gas velocity with respect to the liquid flow. This critical diameter derived from the critical Weber number represents the maximum droplet size which will not experience secondary breakup.

As mentioned previously, the size of the droplets generated from the first mode of entrainment is hard to measure due to the small volume concentration; however, some qualitative estimations can be obtained from previous investigations. Because roll-wave entrainment typically occurs when the wick structure is fully flooded and subjected to increased air/vapor velocities, irregular three-dimensional roll waves are established at the liquid vapor interface. The stability of this wavy surface may be affected by the interaction of two major forces, the surface tension forces which tend to stabilize the interface and the viscous drag forces which tend to destabilize it due to the longitudinal pressure variations. These pressure variations which are lowest at the wave crest, combined with the surface tension, which increases as the crest is approached, cause a liquid bulge to form and become detached by the gas stream (Ishii and Grolmes, 1975).

Tatterson et al. (1977) measured mean droplet sizes for the first mode of entrainment using an electric probe and proposed a semi-empirical correlation based upon the Kelvin-Helmholtz mechanisms. Kataoka et al. (1983) established a semi-empirical correlation to predict the entrained droplet size for roll-wave entrainment. At the instant prior to entrainment, the force balance on the liquid ligament can be expressed as

$$\pi d \sigma = C_d \frac{\pi}{4} d^2 \frac{\rho_v U_r^2}{2} \tag{10}$$

where d is the characteristic diameter, and C_D is the drag coefficient at the wave crest. Introducing the previously developed expression for the Weber number, $We \equiv \rho^v U_r^2 d / \sigma$, this expression can be simplified to yield

$$\mathrm{We} = 8 / C_D \tag{11}$$

where C_D can be obtained from the interfacial shear stress derived by Wallis (1969) through a comparison with experimental data. Thus, the critical Weber number based upon the volume median diameter, d_{md}, is reduced to

$$We_{crit} = 0.01\,\mathrm{Re}^{2/3}\left(\frac{\rho_v}{\rho_l}\right)^{-1/3}\left(\frac{\mu_v}{\mu_l}\right)^{2/3} \tag{12}$$

where the Reynolds number is based on the hydraulic diameter of the channel. The critical diameter based upon the Sauter mean diameter (SMD) can be obtained using the conversion constant presented by Kataoka et al. (1983), and expressed as

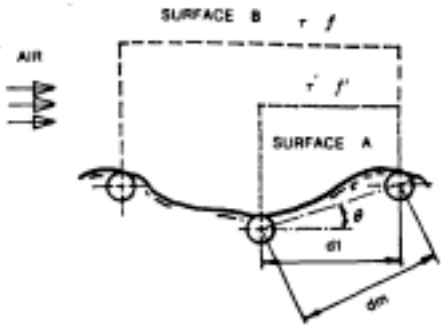

Fig. 2 Control surfaces and local shear stresses

$$d_{pcrit} = 0.00796\frac{\sigma}{\rho_v U_r^2}\mathrm{Re}^{2/3}\left(\frac{\rho_v}{\rho_l}\right)^{-1/3}\left(\frac{\mu_v}{\mu_l}\right)^{2/3} \tag{13}$$

This equation, when compared with the experimental data of Kataoka et a]. (1983), correlates reasonably well and is within a 40-percent error band. These results imply that the gas velocity is the dominant parameter for the roll-wave entrainment mode.

Theoretical Analysis

Investigation of the second mode of entrainment typically begins with a force balance on the control volume illustrated in Fig. 2. Initially, the screen mesh is treated as a series of cyclic surface protuberances, which allow the flow to be idealized as a two-dimensional flow field. In this type of situation, the laminar sublayer of the turbulent duct flow is disturbed by cyclic protuberances (Kays and Crawford, 1980); thus, the corresponding friction factor is several times greater than the values for smooth ducts (Sparrow and Tao, 1983a; 1983b). In addition, the Darcy friction factor can be defined only when the pressure is measured at successive axial locations separated by a distance equal to the pitch of the disturbance elements.

$$f = \frac{(-dp/dX)D_h}{\rho_v U^2} \tag{14}$$

Sparrow and Tao (1983a) indicated that unless the pressures were measured at axial stations with a separation distance equal to the pitch (or from integral multiples of the pitch), significant errors could result. Hence, it was suggested that the friction factor derived from this expression be used to calculate the shear stress, τ, at control surface, B, which corresponds to the pitch of the disturbance element shown in Fig. 2, as

$$\tau = \left(\frac{f}{4}\right)\frac{\rho_v U^2}{2} \tag{15}$$

In examining Fig. 2, it is apparent that in order to obtain a correct estimation of the velocity at which entrainment would occur, it is necessary to obtain not only the skin friction, but also the drag force exerted on the ascending "liquid wall," shown as control surface **A**. Because the surface of control volume **A** does not constitute one pitch of the disturbance element, as suggested by Sparrow and Tao (1983a), the friction factor f' corresponding to the control surface **A** is difficult to determine. However, upon examination, it is clear that the actual value must lie between the smooth wall value and the value derived from the periodic disturbance model.

With this assumption, the total external forces can be balanced with the force resulting from the surface tension occurring in a wick pore with diameter d_m, at the moment of entrainment, or

$$F_\sigma = F_D + F_S \tag{16}$$

$$F_\sigma = \pi d_m \sigma \tag{17}$$

$$F_D = C_D\frac{\rho_v U^2}{2}A_P \tag{18}$$

$$F_S = \left(\frac{f'}{4}\right)\frac{\rho_v U^2}{2}A_S \tag{19}$$

In these expressions, d_m is the harmonic mean of the two principle dimensions, or $\sqrt{d_1^2 + d_2^2}$ which represents there resultant characteristic dimensions in the flow direction, C_D is the drag coefficient, and A_P and A_S are the projected and surface area of the ascerding "liquid wall," respectively. Recognizing that $A_p = (\pi/4)d_m^2 \sin\theta$, where $\sin\theta$ is d_2/d_m and $A_s = (\pi/4)d_m^2$, allows the critical velocity to be expressed as

$$U_c = \left(\frac{8\sigma}{\rho_v(C_D d_2 + (f'/4)d_m}\right)^{0.5} \tag{20}$$

This equation can be nondimensionalized and written in terms of the Reynolds number as

$$\mathrm{Re}_c = \frac{\rho_v D_h}{\mu_v}\left(\frac{8\sigma}{\rho_v d_2(C_D + (f'/4)(d_m/d_2)}\right)^{0.5} \tag{21}$$

where Re_C is the Reynolds number with characteristic dimensions D_h corresponding to the critical velocity. In this expression, D_h is the hydraulic diameter of the channel, and is expressed in the traditional manner. From this expression, the critical velocity can be implicitly determined by numerical computations since both C_D and f' are functions of the Reynolds number and mesh geometry. If the form drag coefficient is assumed to be approximately equal to unity, and the meniscus in control volume B has a convex curvature, and if the surface capillary wave has a very small wavelength compared to the wire spacing (Ishii and Grolmes, 1975), the flow in control volume B may be idealized as flow over a horizontal cylinder.

The form drag coefficient for circular cylinders, C_D, remains constant at a value approximately equal to 1.0 over the Reynolds number range of 10^4 and 10^5 (Schlichting, 1979). For this case, Sparrow and Tao (1983a) established a semi-empirical correlation of the friction factor, f, by modifying the Karman-Nikuradse equation and expressing it as a function of the Reynolds number based on the hydraulic diameter, D_h, the protuberance height to duct hydraulic diameter ratio, d_2/D_h and the pitch to height ratio, d_1/d_2. A roughness function, R^+, was determined by fitting the equation to the experimental data

$$R^+ = 0.685(e^+)^{0.211} \quad , e^+ \le 120 \tag{22}$$

$$R^+ = 1.18(e^+)^{0.015} \quad , e^+ \ge 120 \tag{23}$$

where the roughness Reynolds number, e+ was defined as

$$e^+ = \sqrt{f/8}\left(\frac{d_2}{D_h}\right)\mathrm{Re} \tag{24}$$

and a modified roughness function was defined as the Karman-Nikuradse correlation of the roughness function Re^+, given by

$$R^+ = \left(\frac{d_2}{D_h}\frac{d_1}{d_2}\right)^{1/4}\mathrm{Re}^+ \tag{25}$$

$$R_e^+ = \sqrt{8/f} + 2.5\ln(2d_2/D_h) + 4.23 \tag{26}$$

Using these expressions and the dimensions described and tabulated in Fig. 3, the friction factors for three different mesh sizes have been calculated numerically and compared with those of both a sand-grain roughness model and a smooth wall model. The friction factor, f', for the sand-grain roughness model was calculated from the Karman-Nikuradse equation; i.e.,

$$\frac{1}{\sqrt{f''/8}} = 2.46\ln(D_h/d_2) + 4.22 \tag{27}$$

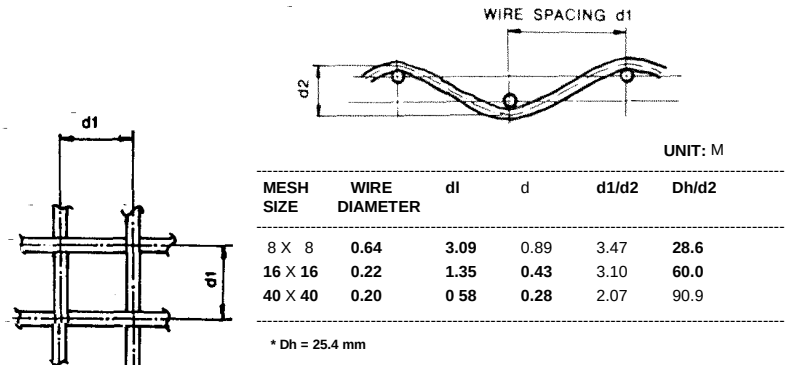

UNIT: M

MESH SIZE	WIRE DIAMETER	dl	d	d1/d2	Dh/d2
8 X 8	0.64	3.09	0.89	3.47	28.6
16 X 16	0.22	1.35	0.43	3.10	60.0
40 X 40	0.20	0 58	0.28	2.07	90.9

* Dh = 25.4 mm

Fig. 3 A detailed configuration and dimensions of copper wire meshes evaluated

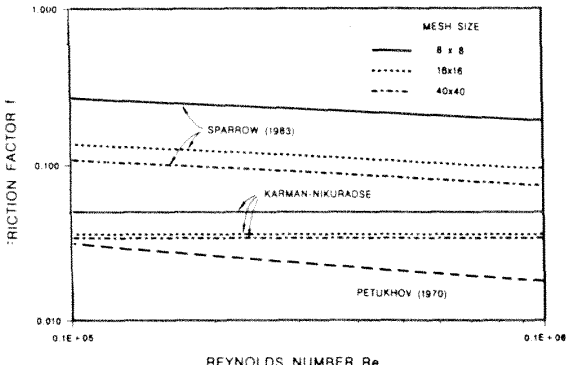

Fig. 4 Comparison of various friction factor models

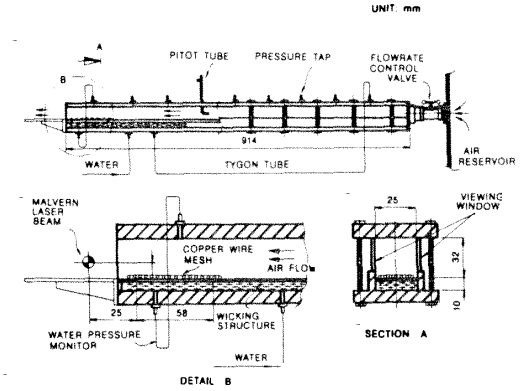

Fig. 5 Detailed configuration and dimensions of the test channel

while the friction factor for a smooth wall, f''', *was* estimated using an equation proposed by Petukhov (1970)

$$f'''/8 = (2.236 \ln Re - 4.693)^{-2} \quad (28)$$

The results of these numerical computations are shown in Fig. *4* as a function of the duct Reynolds number. As illustrated, the friction factor f, for the periodic disturbance model is several times greater than for the value obtained for the smooth wall case, f'''. Thus, as hypothesized previously, f and f''' may constitute an upper bound and a lower bound, respectively, for the actual value of f'.

By eliminating the Reynolds number from both sides of Eq. (21), an expression for the critical Weber number as a function of the characteristic length, d_2, can be written as

$$We_{crit,d_2} = \frac{\rho_v U^2 d_2}{\sigma} = \frac{8}{C_d + (f'/4)(d_m/d_2)} \quad (29)$$

Inspection of this equation, indicates that as the ratio d_m/d_2 increases with increasing mesh dimension, the contribution of f also increases since the friction factor increases with mesh size, as shown in Fig. *4*. This results in a decrease in the critical Weber number or critical velocity; however, the effect of the actual friction factor, f', diminishes as d_m/d_2 approaches unity (for very fine mesh), which implies that the Webe, number converges to $8/C_D$ (similar to the free interface). This new expression includes the effect of the protuberance height, d_2, which has been omitted from previous investigations and analyses.

Experimental Test Description

The experimental portion of the investigation was undertaken to measure the critical velocities corresponding to various mesh sizes in order to verify the criteria proposed for predicting the critical velocity and to establish the SMD variation as a, function of both air velocity and mesh size. To accomplish these two objectives, a test channel similar to the one utilized by Matveev et al. *(1977)* was constructed. The test channel was fabricated in such a way so as to allow the use of laser diagnostic techniques.

As discussed in the literature review, one of the essential conditions for entrainment is a liquid pressure which is high enough to sustain convex menisci and flood the wick structure, at least locally (Prenger and Kemme, *1981).* Preliminary tests indicated that the lowest pressure of the air flow, which is the most favorable situation for entrainment, could be obtained by locating the copper mesh interface at the end of the test channel. A second modification utilized to promote the generation of high-frequency entrainment in the current study was to provide a continuous supply of water so that the entrained sprays would satisfy the minimum volume concentration for a drop-size measurement without depleting the amount of liquid in the wicking structure. This was accomplished by slightly pressurizing the liquid using the upstream air pressure to prevent depletion. These two concepts lead to the development of the heat pipe simulator shown in Fig. 5. This simulator allowed entrainment to take place in a manner similar to that which occurs in a heat pipe, thermosyphon, or other capillarydriven device.

The test channel was fabricated from plexiglass. Two glass viewing windows were inserted in the grooves of the upper wall to allow flow visualization of the menisci and provide optical access of the laser diagnostics. The air flow section of the channel was 25 mm square and approximately 914 mm long, long enough to ensure fully developed flow at the end of the channel where the wicking structure was located. Air flow through the simulator was provided by a large blower and was adjusted by means of a bypass control valve located upstream of the channel. A pitot tube located in the upstream

near the wicked surface was used to measure the flow velocity, and the mean air velocity was calculated using a conversion formula based upon the one-seventh law velocity profile for fully developed turbulent flow.

Nine pressure taps and three water taps were installed along the channel. To insure a continuous supply of water, fifteen layers of copper wire mesh (16 mesh x 16 mesh) were inserted inside of the water chamber. The gap between the top layer of the copper wire mesh and the wicking structure directly under it was designed to be less than 0.5 mm to prevent detachment of the menisci. Water was supplied to the wicking structure through a small tygon tube (3.2 mm inner diameter), and the flow rate was carefully controlled by a manual valve and measured using a standard calibrated rotameter. During the experiment, the water inside of the chamber was under a small amount of pressure generated by an upstream pressure tap, as shown in Fig. 5. In this way, the liquid pressure was maintained slightly higher than the vapor pressure, even at high air velocities. This simulated the flattening of the menisci in the condenser of an actual heat pipe due to condensation of the working fluid. Variation of the liquid pressure below the copper wire mesh was monitored by means of a water pressure monitor, which is shown in Detail B of Fig. 5.

Two parameters were varied during the course of the experiment. First was the air velocity, which was varied from 10 m/s to 64 m/s. This resulted in duct Reynolds numbers of approximately 10^4 to 10^5. Second were the dimensions of the copper wire screen mesh, which had wire spacings ranging from 0.58 mm to 3.09 mm and pitch-to-height ratios from 4 to 7. Water feed rates for each of the various mesh sizes remained fixed throughout the measurement of both the critical velocity and the SMD. To reduce the effect of property variations during the course of the experiment, the temperatures of the air and water were maintained at 25 ^{o}C and 20 ^{o}C, respectively.

Determination of the entrainment onset and measurement of the droplet sizes were accomplished by means of a Malvern 2600 laser sizing system, whose principle of operation is that smaller droplets diffract light at a larger angle than larger droplets, according to Fraunhofer diffraction theory (Barth, 1984). In this way, the Sauter mean diameter, SMD, or d_{32}, which is a mean diameter derived from the ratio of the total volume of an aerosol to its total surface area, could be determined. This value, which can be expressed mathematically as

$$SMD = \frac{\sum_{k=1}^{N} n_i d_{pi}^3}{\sum_{k=1}^{N} n_i d_{pi}^2} \tag{30}$$

is typically used in the analysis of aerosol sprays.

All of the experimental data shown in the drop size measurements were obtained by averaging three SMD measurements and five sweeps were used for each SMD measurement. The resulting five consecutive integrations of the light energy spectrum on the ring diodes were statistically converted into a dropsize distribution. In the current investigation, the SMD measurements utilized the Rosin-Rammler size distribution model, which is typically a better functional form than the log-normal distribution when the skewness of the entrained sprays is large (Hinds, 1982). This model has the functional form

$$Q = 1 - \exp - \left(\frac{d_p}{d_{po}} \right)^q \tag{31}$$

where Q is the volume fraction of particles of diameter less than d_p, and the two model parameters, d_{po}. and q, denote a median and an inverse of the standard deviation of droplet distributions, respectively.

The Malvern laser beam was focused to a diameter of approximately 5 mm, leveled, and then positioned perpendicular to the test channel. The sampling location was 15 mm frorr the end of the channel and the beam centerline was locatec approximately 3 mm above the copper wire mesh. The SME measurements were found to be relatively insensitive to th horizontal location, but extremely sensitive to the vertical position. Thus, several preliminary experiments were performed to determine the vertical location that would provide a maximum data rate.

The Malvern system was modified so that it could be triggered by a spray synchronizer once the obscuration, defined as $(I_o\text{-}I)/I_o$ was greater than a preset reference value. In this expression, the term $(I_o\text{-}I)$ represents the reduction in laser light intensity due to the presence of the aerosol, and I_o represents the intensity without any aerosol present. This sprays synchronizer was interfaced with the Malvern laser sizer to allow measurement of the SMD for the unsteady entrained sprays. More description on the principle and development of the obscuration synchronization technique has been presented by Kihm and Caton (1992). Aerosols generated from the menisci formed in the copper wire mesh scattered the laser light and triggered the synchronizer to detect the light, which was then detected by the ring diode.

As noted, the spray synchronizer was interfaced with the Malvern receiver to detect the center diode voltage as a measure of the obscuration. Using a voltage control dial, the trigge voltage could be set to the desired level. As the volume con centration of the intermittently entrained sprays increased, the corresponding spray obscuration exceeded a reference value set by the reference voltages. At this point, the Malvern system was triggered and the SMD measurements were made. The procedure was repeated for each sweep triggered by each in termittent spray.

The alignment of the Malvern instrumentation was adjusted to within ± 2 percent using a standard calibrating reticle, and the standard deviation of the data fitting process used on the detected light energy was maintained to within ± 5 percent. This resulted in an overall uncertainty of the SMD measurements of less than ±10 percent.

Results and Discussion

The quantitative experimental results can be divided into two major sections: (*i*) measurements of the critical velocities for the different mesh sizes, and comparison with those derived from the theoretical criteria; and (*ii*) measurement of the SMD of the entrained droplets as a function of the mesh size and air velocity, and the development of a dimensionless expression for predicting the mean drop size.

Critical Velocity Measurements. The lower and upper critical velocities, illustrated in Fig. 6, correspond to the measured onset velocities for the first and second modes of entrainment, respectively. Figure 6 shows an interesting trend in the behavior of the two critical velocities. Increases in the mesh dimension decreased both the upper and lower critical velocities and increased the size of the transition region between the two modes. For smaller mesh sizes, the size of the transition region tended to diminish, as did the difference in the critical velocity for the two modes.

It is important to note that for small mesh sizes, the lower critical velocity was determined visually by the laser-light scattering method, and the upper critical velocity was determined by detecting the increase in aerosol concentration at the onset of the second mode of entrainment through the obscuration measurement. Because the Malvern system requires a minimum threshold concentration, and for large mesh sizes, the upper critical velocities were more difficult to define since there was not as large an increase in the aerosol concentration, the onset of the second mode of entrainment for larger screen meshes may actually occur at a somewhat lower velocity than reported

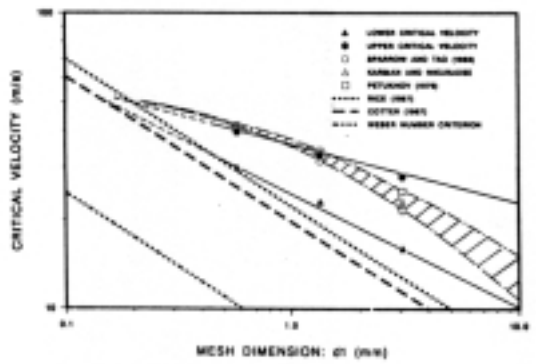

Fig. 6 Critical velocities as a function of mesh dimensions

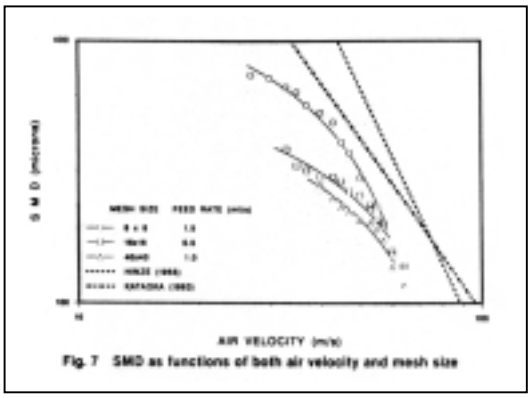

Fig. 7 SMD as functions of both air velocity and mesh size

Figure 6 also illustrates comparisons between the previously developed analytical methods for predicting the onset of entrainment and shows that the critical velocities derived using the method proposed by Cotter (1967), Eq. (3), as well as those resulting from the method proposed by Rice and Fulford (1987), Eq. (7), are reasonably close for small mesh dimensions, but not as accurate for larger mesh sizes. These results imply that the Rice and Fulford, and the Cotter criteria derived from surface instability theory can more closely estimate the critical velocity for the first mode of entrainment or lower critical velocity. This is especially true for the case of the critical Weber number criteria, which appears to significantly underestimate the experimental data. (These theories were established for the case of a free interface rather than an intermittently interrupted surface.)

Extrapolation of the upper and lower critical velocities constitutes a region in Fig. 6, which merges together at a mesh dimension or wire spacing of approximately 0.1 mm. The lower critical velocity results agree quite well with the predictions of Rice et al. (1987) and Cotter (1967) when the pore diameter is less than approximately 0.6 mm. In other words, the criteria based upon instability of a free interface can be effectively applied to estimate only the lower critical velocities of wicked interfaces if the capillary wavelength of the liquid within the capillary pores is smaller than the pore diameter of a wick, as suggested by Busse and Kemme (1980). As noted earlier, Matveev et al. (1977) performed an experimental investigation to evaluate the validity of the Cotter criterion, using screen mesh sizes with a capillary pore diameter of less than 0.6 mm. The results of that experimental investigation also showed good agreement with the values predicted using the criterion of Cotter.

Figure 6 also shows the upper critical velocities obtained using the three friction factor models (f, f'' and f''') and Eq. (20). As illustrated, the upper critical velocity decreases with increases in the mesh dimension. One explanation is that, as seen in Eq. (20) and illustrated in Fig. 4, the effect of skin friction on the critical velocities is considerably greater for larger mesh sizes, whereas it is negligible for the smaller ones.

The predictions shown in the hatched region of Fig. 6 are nearly the same and very close to the actual upper critical velocity for the case of small meshes whose wire spacing, d_1, is less than or equal to 1.0 mm. With further increases in the mesh dimension, the critical velocities obtained from the theoretical criterion decrease and deviate more from the experimentally measured upper critical velocities. In addition, the prediction shows that the actual critical velocity may exist in the hatched region bounded by the two critical velocities obtained using the Sparrow and Tao (1983) friction factor, f, and the lower critical velocity obtained using the friction factor, f''', proposed by Petukhov (1970).

SMD Measurements. In the second phase of the experimental investigation, a parametric study of the droplet size distribution was conducted. The results of this phase are shown in Fig. 7 as a function of air velocity for the three different mesh sizes described in Fig. 3. The SMD measurements were made for the second mode of entrainment sprays, while available correlations of SMD were only for the first entrainment mode. As illustrated, all of the SMD data for the second mode of entrainment are smaller than the critical diameters for the given velocities obtained using the expression derived by Hinze (1955). This implies that most of the droplets generated from the primary disintegration of the ligaments are not subjected to secondary breakup. This observation also indicates that the primary droplet generation mechanism for the second mode of entrainment is not secondary breakup, but entrainment due to ligament disintegration. The SMD values for the first mode of entrainment by Kataoka et al. (1983) are also smaller than the critical diameters predicted by Hinze (1955) for lower air velocities, but, as shown in Fig. 7, the two lines merge together at approximately 70 m/s. Similarly, droplets generated by the first mode of entrainment are not influenced by secondary breakup, again indicating that entrainment is the dominant droplet generating mechanism occurring in this investigation.

With increases in the mesh dimension, the experimental results for the second mode of entrainment tends to approach the values predicted by Kataoka et al. (I 983), but do not exceed the predicted values, even for meshes with a capillary pore radius of 3.09 mm. This may indicate that the wicked interface results in droplet generation mechanisms other than "roll-wave entrainment," and produces droplets with diameters comparable to the diameters of the ligaments by "elongated ligament entrainment."

Figure 7 also shows the effect of air velocity on the SMD variation. For low air velocities near the onset of the second mode of entrainment, the rate of SMD decrease is nearly the same for all three mesh sizes. However, as air velocity increases, the rate of decrease for the large mesh size (8 x 8), i.e., d_1 = 3.09 mm, is significantly greater than for the other two sizes. It is also interesting to note that the three curves merge together at a velocity of approximately 70 m/s. This implies that the thicker ligaments generated by larger mesh sizes may be subjected to more severe stretching because of the higher air velocity, diminishing the dependence of SMD on the mesh dimension. To illustrate the effect of the mesh dimensions on the droplet diameter, the SMD was plotted as a function of the wire spacing for several different air velocities. As indicated in Fig. 8, the wire spacing has little effect on the SMD variation for high velocities; however, as the air velocity decreases, the impact of mesh diameter becomes more important.

The droplet generation mechanism for the second mode of entrainment can be interpreted using the stability diagram of

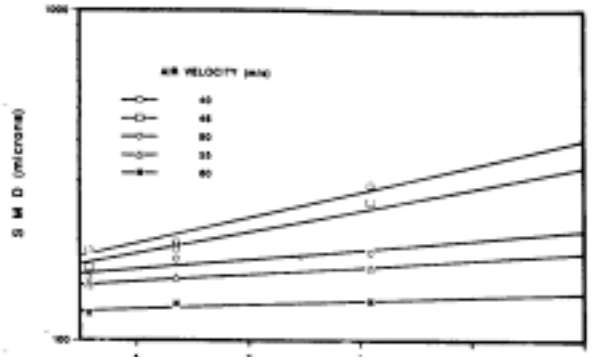

Fig. 8 SMD as a function of the mesh size for the given air velocities

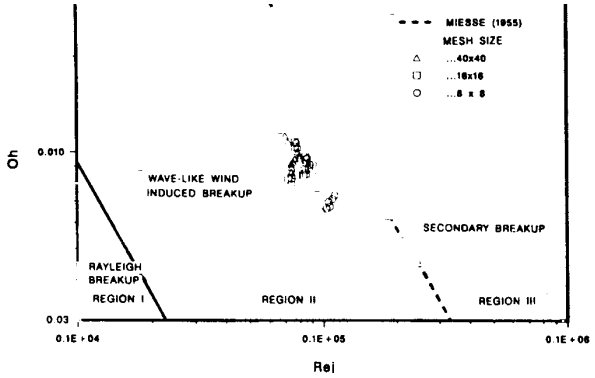

Fig. 9 Ohnesorge number as a function of the jet Reynolds number for the three mesh sizes

liquid jets proposed by Ohnesorge (1936). Figure 9 compares the Ohnesorge number as a function of the jet Reynolds number. As shown, none of the data obtained are in the region of "secondary breakup," but in a region where the elongated ligaments are held on by the meniscus and subjected to violent wavy undulations and air friction.

At the beginning of entrainment, the largest mesh displayed a lower Ohnesorge number than the others, implying that the larger ligaments tend to be maintained longer. As a result, the droplets may not be as fine as for the finer meshes due to the relatively large surface tension to air friction ratio. Figure 9 also indicates that the Ohnesorge numbers of the jets increase and merge together as the air velocity increases. However, it is important to note that the Reynolds numbers based on the droplet diameter decrease even for increasing air velocity, due to the faster reduction of ligament diameters, which also results in faster reduction of droplet diameters. This supports the merging of the SMD curves in Fig. 8, since the breakup distance becomes identical with increases in the air velocity.

Because the water feed rate can affect the curvature of the meniscus, an additional series of tests was conducted to determine how variations in the water feed rate affected the SMD. The results indicated that the SMD values were relatively insensitive to variations in the water feed rate, provided the wick structure was properly primed. The only time water feed rate influenced the droplet size or formation was when the feed rate was not high enough to properly prime the menisci.

Based upon a parametric study of SMD variation, three independent dimensionless terms and one dependent dimensionless term can be introduced to characterize the functional relationship between the parameters. The Weber number can be used as a dependent term to represent the droplet diameter,

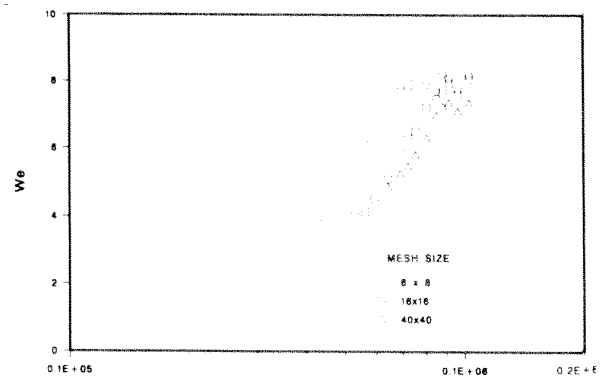

Fig. 10 Weber number as a function of the Reynolds number for the three mesh sizes

d_1/d_2, D_h/d_2 and the Reynolds number as independent terms This results in a functional relationship of the form

$$\mathrm{We} = f(\mathrm{Re}, d_1/d_2, D_h/d_2) \tag{32}$$

where

$\mathrm{We} = \rho_v U^2 d_p / \sigma$

$\mathrm{Re} = \rho_v U D_h / \mu_v$

d_1/d_2 = pitch to height ratio of meshes

D_h/d_2 = duct hydraulic diameter to height ratio

In order to derive the empirical correlation, the Weber numbers for the experimentally obtained SMD values were plotted in Fig. 10 as a function of the Reynolds number that represents the nondimensionalized mesh dimensions. The results indicate that the Weber number increases with increases in Reynolds number, but that this increase diminishes and tends to remain unchanged when the Weber number reaches a value of approximately eight. This implies that two different functional relationships exist between the Weber number and Reynolds number for each mesh, one which is mesh dependent and one which is mesh independent.

In the mesh-dependent region, the Weber number is a function of both the Reynolds number and the mesh geometry, while in the mesh-dependent region, the Weber number remains nearly constant regardless of the mesh dimensions. In addition, for a fixed Reynolds number, the Weber number tends to increase with increases in d_1/d_2, but decreases with increases in D_h/d_2. Physically, this trend is quite reasonable since large droplets can be obtained by increases in wire spacing and smaller droplets are generated as d_2 decreases. However, the combined effect of the two dimensionless parameters on the SMD variation has more significance than just the individual contributions, making both parameters necessary to completely define the effect of the mesh geometry.

For the mesh-dependent region, the Weber number can be expressed as

$$\mathrm{We} = c_1 \mathrm{Re}^x (d_1/d_2)^y (D_h/d_2)^z \tag{33}$$

If all three sets of experimental data are substituted into this expression, the four unknown coefficients can be determined using a least-squares approximation method. The resultant correlation for the SMD variation is

$$We = 1.0965 \times 10^{-4}\, \mathrm{Re}^{1.166} \left(\frac{d_1}{d_2}\right)^{-0.276} \left(\frac{D_h}{d_2}\right)^{-0.448} \tag{34}$$

This correlation illustrates the dependency of the Weber number on the Reynolds number. Initially, the negative exponent on d_1/d_2 appears to contradict the experimental results since the Weber number decreases with increases in d_1/d_2. However, the decrease is more than compensated for by the increase in

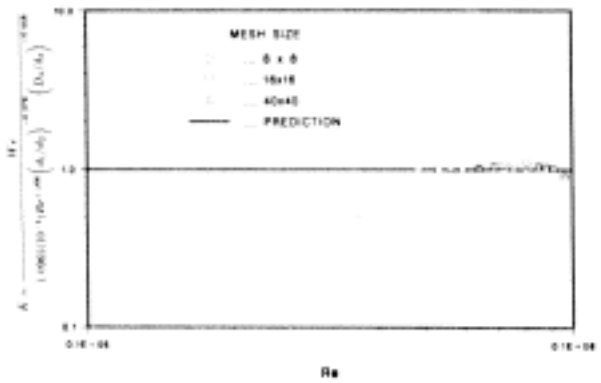

Fig. 11 Parameter K as a function of the Reynolds number for both experimental data and the empirical correlation

$(D_h/d_2)^{-0.448}$; hence, the Weber number increases with increasing d_1/d_2. If a new parameter is introduced

$$K = \frac{We}{1.09651\times10^{-4}\,\mathrm{Re}\left(\frac{d_1}{d_2}\right)^{-0.276}\left(\frac{D_h}{d_2}\right)^{-0.448}} \tag{35}$$

the effect of all the dimensionless parameters can be seen. The results can be plotted as a function of the Reynolds number, as shown in Fig. 11, and show good agreement between the experimental data and the empirical correlation, with values within approximately ±10 percent.

Conclusions

An experimental investigation was conducted to identify and better understand the parameters that govern the entrainment of liquid droplets in high-velocity air/vapor streams flowing over screen mesh interfaces in heat pipes and other capillary pumped systems. Using a flow visualization technique, two modes of entrainment were identified and described for highvelocity gas flows over an intermittently interrupted liquid surface. These two modes, roll-wave entrainment and stripping entrainment, were found to correspond to the lower and upper critical gas velocities, respectively. The first mode of entrainment was found to occur when the capillary wicking structure was fully flooded. The second mode of entrainment was observed only at higher air velocities and only when the liquid pressure was high enough to produce a convex meniscus shape with the mesh primed properly.

Measurements of the critical air velocity and the droplet size distribution (Sauter mean diameter) of the entrained sprays were also made as a function of the capillary pore size for three different mesh sizes and the results were compared with the analytical models developed in several previous investigations. The flow visualization and experimental results both indicate that the upper critical velocity is insensitive to the variation of water feed rate as long as the capillary pores are properly primed. The upper and lower critical velocities were observed to merge together as the mesh dimensions decreased and good agreement was obtained with previously develope~ analytical models, particularly those of Cotter (1967) and Rice and Fulford (1987), provided d, is smaller than 0.3 mm. The difference between the upper and lower critical velocities was found to be magnified with increased mesh size. New theoretical criteria, Eqs. (20) and (21), were shown to predict the upper critical velocity accurately for a wide range of mesh dimensions, and a critical Reynolds number which corresponded to the critical velocity was also proposed. Based upon a parametric study, an empirical correlation to predict SMD has been developed and presented and shows good agreement with the experimental data.

The major droplet generation mechanism was shown to not be the result of secondary breakup, but by entrainment resulting from ligament disintegration induced by surface waves and viscous friction. Finally, the air velocity and mesh dimensions were shown to be the most significant parameters in determining the SMD variation; however, the effect of mesh dimension, while distinct for lower air velocities, diminished with increases in the air velocity.

Acknowledgment

Support for this investigation was provided by the National Science Foundation through Grant No. CTS-8922427.

References

Barth, H. G., 1984, *Modern Method of Particle Size Analysis,* John Wiley and Sons, New York, NY, pp. 135-172.

Brodkey, R. S., 1967, *The Phenomenon of Fluid Motion,* Addison-Wesley, New York, NY, pp. 112-115.

Busse, C. A., and Kernme, J. E., 1980, "Dry-out Phenomena in GravityAssisted Heat Pipes with Capillary Flow," *International Journal of Heat and Mass Transfer, Vol.* 23, pp. 634-654.

Cotter, T. P., 1967, "Heat Pipe Startup Dynamics," *Proceedings, SAE Thermionic Conversion Specialist Conference,* Palo Alto, CA, pp. 344-347.

Hinds, W. C., 1982, *Aerosol Technology,* John Wiley and Sons, New York, NY, pp. 97-98.

Hinze, J. 0., 1955, "Fundamentals of the Hydrodynamic Mechanism of Splitting in Dispersion Process," *AlChE Journal,* Vol. 1, pp. 289-295.

Ishii, M., and Grolmes, M. A., 1975, "Inception Criteria for Droplet Entrainment in Two-Phase Concurrent Film Flow," *AlChE Journal, Vol.* 21, pp. 308-318.

Kataoka, L, Ishii, M., and Mishima, K., 1983, "Generation and Size Distribution of Droplets in Annular Two-Phase Flow," ASME *Journal of Fluids Engineering, Vol.* 105, pp. 230-238.

Kays, W. M., and Crawford, M. E., 1980, *Convective Heat andMass Transfer,* McGraw-Hill, New York, NY, pp. 197-202.

Kihm, K. D., and Caton, J. C., 1992, "Synchronization of a Laser Frauhofer Diffraction Drop Sizing Technique with Intermittent Spray System," *Applied Optics, Vol.* 31, pp. 1914-1916.

Lamb, H., 1945, *Hydrodynamics,* Chap. IX, Dover Press, New York, NY, pp. 430-438.

Lane, W. R., 1951, "Shatter of Drops in the Streams of Air," *Industrial Engineering Chemistry,* Vol. 43, pp. 1312-1317.

Matveev, V. M., Filippov, Y. N., Dyuzhev, V. I., and Okhapkin, E. V., 1977, "Breakaway of a Liquid by a Gas Stream at an Interface Containing Grid," *Journal of Engineering Physics, Vol.* 33, pp. 1008-1012.

Ohnesorge, W., 1936, "Formation of Drops by Nozzles and The Breakup of Liquid Jets," *Mathematics ofMechanics,* Vol. 16, pp. 355-358.

Peng, X. F., Peterson, G. P., and Wang, B. X., 1992, "Capillary Induced Rewetting in a Flat Porous Cover Layer," *International Journal of Heat and Mass Transfer, Vol.* 35, No. 2, pp. 319-328.

Peterson, G. P., 1986, "Thermal Control Systems For Spacecraft Instrumentation," *AIAA Journal ofSpacecraft and Rockets,* Vol. 24, No. 1, pp. 714.

Peterson, G. P., and Bage, B., 1991, "Entrainment Limitations in Thermosyphons and Heat Pipes," ASME Journal of Energy Resources Technology, Vol. 113, pp. 147-154.

Petukhov, B. S., 1970, *Advances in Heat Transfer,* Academic Press, New York, NY, pp. 503-504.

Prenger, F. C., and Kemme, J. E., 1981, "Performance Limits of GravityAssisted Heat Pipes with Simple Wick Structures," *Proceedings, 41h International Heat Pipe Conference, pp.* 137-146.

Rice, G., and Fulford, D., 1987, "Influence of a Fine Mesh Screen on Entrainment in Heat Pipes," *Proceedings, 6th International Heat Pipe Conference,* pp. 168-172.

Richardson, S. M., 1989, *Fluid Mechanics,* Hemisphere Publishing Co., New York, NY, pp. 260-266.

Schlichting, H., 1979, *G~andary-Layer Theory,* McGraw-Hill, New York, NY, p. 17.

Sparrow, E. M., and Tao, W. Q., 1983a, "Enhanced Heat Transfer in a Flat Rectangular Duct with Streamwise-Periodic Disturbances at One Principal Wall," ASME *Journal of Heat Transfer,* Vol. 105, pp. 851-861.

Sparrow, E. M., and Tao, W. Q., 1983b, "Symmetric vs Asymmetric Periodic Disturbances at the Wall of a Heated Flow Passage," *International Journal of Heat Mass Transfer, Vol.* 27, pp. 2133-2143.

Tatterson, D. F., Dallman, J. C., and Hanratty, T. J., 1977, "Drop Sizes in Annular Gas-Liquid Flows," *AIChE Journal,* Vol. 23, pp. 68-76.

Wallis, G. B., 1%9, *One-Dimensional Two-Phase* Flow, McGraw-Hill, New York, NY, pp. 345-351 and 376-391.